JOC The Journal of Organic Chemistry

Article

pubs.acs.org/joc

Solution-Phase Dimerization of an Oblong Shape-Persistent Macrocycle

Meng Chu, Ashley N. Scioneaux, and C. Scott Hartley*

Department of Chemistry & Biochemistry, Miami University, Oxford, Ohio 45056, United States

Supporting Information

ABSTRACT: A new shape-persistent macrocycle comprising two 2,3-triphenylene moieties bridged by *m*-phenylene ethynylenes has been synthesized. UV−vis and fluorescence spectroscopies indicate limited interaction between the two triphenylene units. The compound, which has a pronounced oblong shape (the core measures approximately 2.2 × 1.0 nm), aggregates in $CDCl_3$ and toluene-d_8 to give stacked dimers, as indicated by the ^{1}H NMR signals corresponding to protons on or near the core, which shift upfield with increasing concentration. These changes in NMR shielding were modeled using DFT calculations on candidate dimer geometries. The best match to the experimental data was obtained for a dimer consisting of arene−arene stacking by 3.6 Å (on average) with a displacement along the molecular long axis of 3.5−4.0 Å. This displacement is larger than can be explained by the electronic effects of aromatic stacking interactions. Instead, the minimization of steric interactions between the side chains appears to control the dimer geometry, with the alkoxy groups of one molecule sliding into registry with the gaps along the periphery of the other. Such lateral displacement (as opposed to rotation) is a direct consequence of the extended oval shape of the compound.

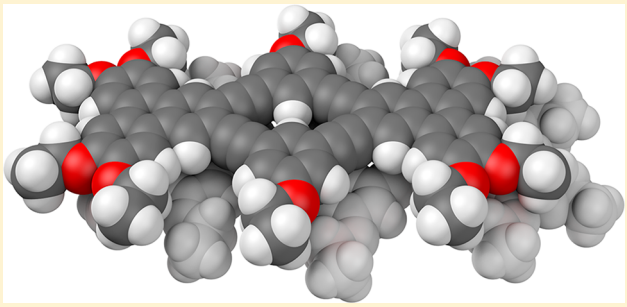

INTRODUCTION

The self-assembly of disc-shaped molecules into columns is important in the generation of functional materials, as has been demonstrated, for example, in self-assembled nanostructures,[1] gels,[2] and discotic liquid crystals.[3,4] Often, the formation of these supramolecular structures is driven by the stacking of shape-persistent aromatic cores, leading to functional properties through intermolecular charge and energy transfer. Related to these bulk materials, the solution-phase aggregation of disc-shaped molecules into dimeric or polymeric stacks provides important model systems for understanding aromatic stacking and is also used to generate systems with useful properties.[5−7] In this context, many structural classes have been explored,[5] including polycyclic aromatics (e.g., triphenylenes,[8] hexabenzocoronenes,[9] and perylene diimides[10]) and shape-persistent macrocycles.[11−14]

Recently, we have been exploring the properties of a new class of shape-persistent macrocycles with push−pull designs, focusing on functionalized tetrabenzo[18]cyclynes (TBCs) and related structures.[15,16] Our previously reported compounds feature electron-rich and -poor units separated by pairs of (cross-)conjugated bridges (i.e., they are donor−bridge−acceptor compounds with two bridges). These macrocycles represent a simple, fundamental design for two-dimensional π systems, allowing the study of electron transfer mediated by multiple conjugated pathways. Our focus to this point has been the spectroscopic investigation of single-molecule properties; however, a long-term goal of the project is the incorporation of these chromophores into functional materials through columnar stacking (e.g., in liquid crystals). The stacking of discotic molecules through arene−arene interactions is, of course, well-known. However, the push−pull macrocycle design has a subtle but important structural consequence for self-assembly: by their nature, these structures will have oblong shapes on nanometer-length scales, unlike the majority of discotics which are approximately circular. While examples of similar structures are known (discussed below), to the best of our knowledge the consequences of an oblong shape on the stacking geometries of nm-scale discotics have not been examined in detail.

Here, we present the synthesis, characterization, and aggregation properties of a new shape-persistent macrocycle, **Tp(mP)$_2$Tp**. This compound allows us to probe two new elements of our TBC design: the electronic communication between relatively large chromophores (triphenylenes) as mediated by the *m*-phenylene bridges and the effect of the extended, oval-like shapes on aromatic stacking. An important feature of **Tp(mP)$_2$Tp** is that it exhibits clean dimerization in solution which is readily monitored by ^{1}H NMR spectroscopy. Consequently, it is a useful model system for the study of solution-phase aromatic stacking, particularly as DFT calculations of the changes in ^{1}H NMR chemical shifts allow the dimer geometry to be determined directly.

Compound **Tp(mP)$_2$Tp** complements recent reports of triphenylene-containing macrocycles, which have featured the triphenylene moieties connected at the 3,6 positions (as

Received: June 5, 2014
Published: September 3, 2014

   dx.doi.org/10.1021/jo501260c | J. Org. Chem. 2014, 79, 9009−9017

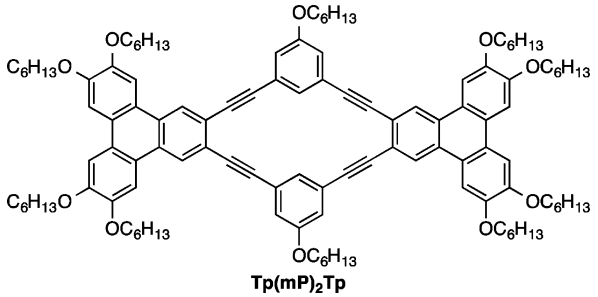

opposed to 2,3). For example, Peng has used bridged triphenylene macrocycles as rigid core units in the self-assembly of microstructures, also exploring their photophysical properties,[17−19] including one example with a core that is isomeric with that of **Tp(mP)$_2$Tp**.[18] Likewise, Cammidge has examined bridged triphenylenes as a design paradigm for discotic nematic liquid crystals[20] and as porphyrin-like architectures.[21] Other triphenylene-based macrocycles have been explored for their spectroscopic properties and self-assembly on surfaces, in solution, and in the bulk.[22,23]

RESULTS AND DISCUSSION

Synthesis. Our synthesis of **Tp(mP)$_2$Tp**, shown in Scheme 1, is based on our previously reported strategy toward push−pull macrocycles. Briefly, known 2,3,6,7-tetramethoxytriphenylene[24,25] was brominated to give **2**, which was subsequently deprotected to give 2,3-dibromo-6,7,10,11-tetrahydroxytriphenylene **3**. Surprisingly, despite its structural simplicity and its potential as an advanced precursor to desymmetrized triphenylenes (e.g., for liquid crystals[25−27]), compound **3** does not appear to have been previously reported. Alkylation of **3** gave known[25] intermediate **4**, which was coupled with the *m*-phenylene bridges[28] by standard Sonogashira coupling to give compound **Tp(mP)$_2$**, a useful reference compound for later comparison of its properties to those of **Tp(mP)$_2$Tp**. The key macrocyclization step using copper-free Sonogashira coupling conditions with Pd(P^tBu_3)$_2$ as the catalyst[29] gave the target compound in modest yield (16%). This yield is lower than was achieved for our previous macrocycles[15,16] but is explained by the use of less efficient aryl bromide substrate **4** in the present case as opposed to more reactive aryl iodides.

Scheme 1[a]

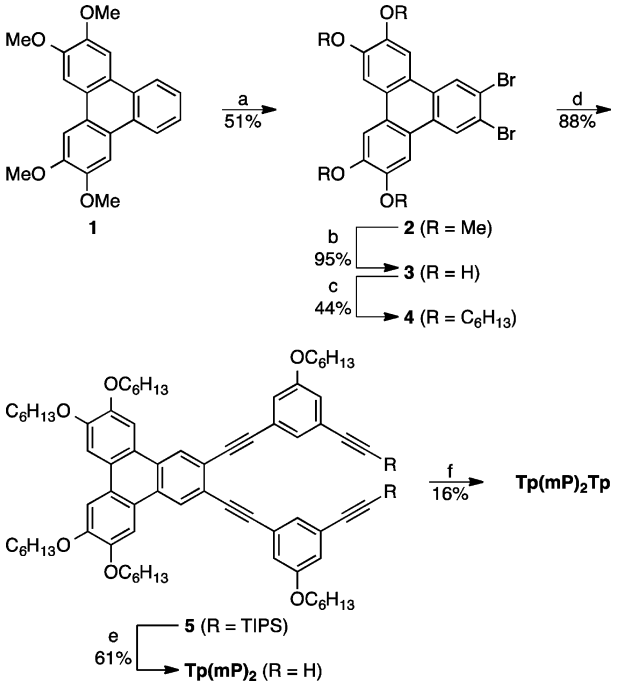

[a]Reagents and conditions: (a) Br_2, CH_2Cl_2, rt; (b) BBr_3, CH_2Cl_2, rt; (c) $C_6H_{13}Br$, K_2CO_3, DMF, reflux; (d) 1-ethynyl-3-(hexyloxy)-5-(triisopropylsilylethynyl)benzene, $Pd(OAc)_2$, CuI, PPh_3, NEt_3, toluene, 80 °C; (e) TBAF, THF, rt; (f) **4**, Pd(P^tBu_3)$_2$, NEt_3, toluene, rt.

To better understand its structure, macrocycle **Tp(mP)$_2$Tp** was studied by DFT calculations at the B3LYP/6-31G(d) level, with the hexyloxy groups simplified to ethoxy groups (**Tp(mP)$_2$Tp′**). The optimized geometry is shown in Figure 1. At this level of theory, the C_2-symmetric macrocycle is very close to planarity, with a slight distortion from perfect C_{2h} symmetry. The intraannular hydrogen atoms are predicted to be only 2.12 Å apart, slightly below the sum of their van der Waals radii (2.18 Å). The width of the macrocyclic core is approximately 1.0 nm and its length is 2.2 nm as measured between opposing carbon atoms (Figure 1). As shown in the Supporting Information, the calculated HOMO of the macrocycle is predicted to be localized on the triphenylene moieties, whereas the LUMO is localized on the *m*-phenylene bridges. For comparison, similar calculations were also performed for the acyclic precursor **Tp(mP)$_2$**, again with the hexyloxy groups simplified to ethoxy groups (**Tp(mP)$_2$′**, see the Supporting Information). To best correspond to the structure of the macrocycle, we only considered the conformer with the alkynyl hydrogens directed inward. Not surprisingly, the geometry of this reference structure is distorted from planarity because of steric interactions between the alkynyl groups, with each *m*-phenylene unit twisted by 19° from the plane of the triphenylene. The FMOs, however, are directly analogous to those calculated for **Tp(mP)$_2$Tp′**.

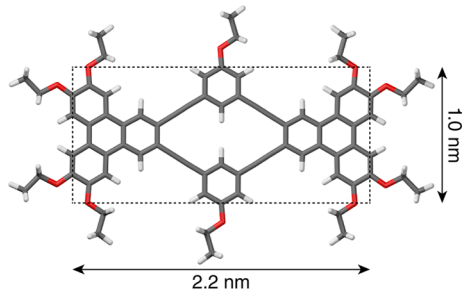

Figure 1. Optimized geometry of **Tp(mP)$_2$Tp′** (B3LYP/6-31G(d)).

Photophysical Properties. We were interested in investigating whether the cross-conjugated *m*-phenylene bridges mediate electronic communication between the triphenylenes. UV−vis and fluorescence spectra of both **Tp(mP)$_2$Tp** and **Tp(mP)$_2$** are shown in Figure 2.[30] TD-DFT calculations on **Tp(mP)$_2$Tp′** at the ground-state geometry are in good agreement with the UV−vis spectrum of **Tp(mP)$_2$Tp** (see the Supporting Information). To further probe the photophysical properties of the compounds, quantum yields (Φ) and fluorescence lifetimes (τ) were also determined and are shown in Table 1. From these values, radiative ($k_r = \Phi\tau^{-1}$) and nonradiative ($k_{nr} = (1 - \Phi)\tau^{-1}$) rate constants for excited-state decay were calculated.

dx.doi.org/10.1021/jo501260c | J. Org. Chem. 2014, 79, 9009−9017

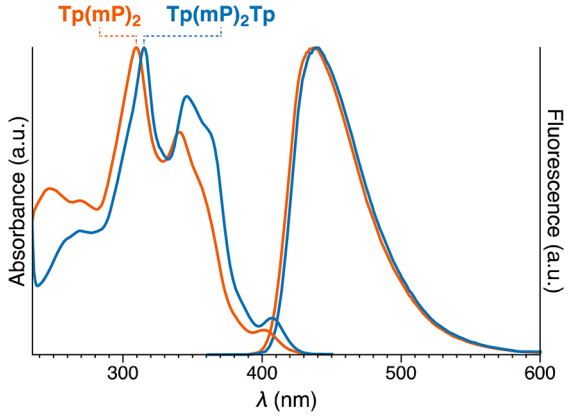

Figure 2. UV−vis and fluorescence spectra of **Tp(mP)$_2$Tp** and **Tp(mP)$_2$** in CH_2Cl_2 (1.0×10^{-6} M and 5.0×10^{-7} M, respectively).

Table 1. Photophysical Properties of Tp(mP)$_2$Tp and Tp(mP)$_2$ in CH_2Cl_2

compd	Stokes shift (nm)	Φ	τ^a (ns)	k_r (ns^{-1})	k_{nr} (ns^{-1})
Tp(mP)$_2$Tp	33	0.62	5.2	0.12	0.073
Tp(mP)$_2$	37	0.55	5.7	0.096	0.079

[a]Monoexponential fits obtained in both cases.

The similarities in the UV−vis and fluorescence properties of the two compounds suggest no significant interaction between the triphenylenes in either the ground or excited states, with only small effects that can be rationalized by constraints imposed by macrocyclization. The small differences in Stokes shifts, quantum yields, and fluorescence lifetimes likely result from a smaller degree of excited-state geometric reorganization, a small decrease in the nonradiative excited-state decay rate (k_{nr}) because of structural rigidity, and a small increase in the radiative excited state decay rate (k_r) because of enforced planarization of the π-system.[31] This behavior is in contrast to that recently observed for a triphenylene dimer macrocycle bridged by butadiyne units at the 3,6 positions, for which increased ground-state conjugation but decreased excited-state conjugation were observed because of strain imposed by the macrocyclic structure.[23] The similarity in photophysical properties between **Tp(mP)$_2$Tp** and **Tp(mP)$_2$** is consistent with the very low strain of the tetrabenzo[18]cyclyne core and the cross-conjugated nature of the *m*-phenylene bridges.

Solution-Phase Aggregation. Macrocycle **Tp(mP)$_2$Tp** exhibits concentration-dependent ^{1}H NMR spectra in $CDCl_3$ and toluene-d_8,[32] with pronounced upfield shifts of the signals associated with the protons on or near the rigid core. This phenomenon is commonly attributed to aggregation through the stacking of aromatics, with the upfield shifts resulting from the placement of protons in the shielding zone above the neighboring aromatic system. The chemical shifts, shown in Figure 3, were well fit by a monomer−dimer equilibrium model[33]

$$\delta = \Delta\delta\left(1 + \frac{1 - \sqrt{8K_dC + 1}}{4K_dC}\right) + \delta_m \quad (1)$$

where δ is the observed chemical shift, $\Delta\delta$ ($= \delta_d - \delta_m$) is the overall change in chemical shift from monomer (δ_m) to dimer (δ_d), C is the concentration, and K_d is the association constant for dimer formation. This model cannot in itself distinguish a

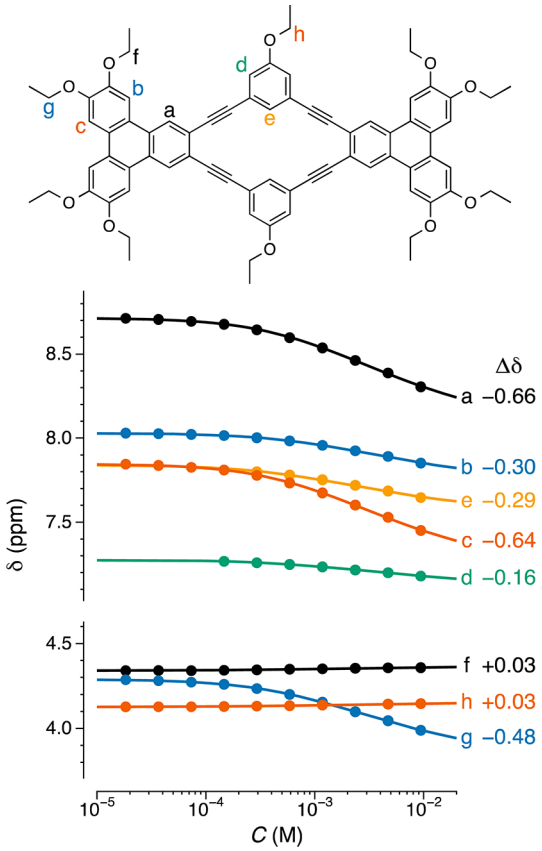

Figure 3. Observed NMR shifts (δ) as a function of concentration (C) in $CDCl_3$. The solid lines are fits to eq 1, the $\Delta\delta$ are those extracted from the fits.

monomer−dimer equilibrium from polymerization by isodesmic indefinite association.[34] However, the overall changes in δ are consistent with aggregation that predominantly stops at the dimer ($\Delta\delta$ < 1 ppm).[33] Strong additional support for dimerization is obtained from the DFT calculations of $\Delta\delta$ described below, which indicate that the shielding effect of two (and only two) stacked molecules accounts for the observed spectral changes.

Nonlinear least-squares fits of eq 1 (Figure 3) to the experimental data yielded values for K_d, δ_m, and δ_d (and thus $\Delta\delta$). The association constants K_d are in good agreement regardless of which proton signal is considered. Taking the (variance-weighted) average, we obtain $K_d = 215 \pm 5$ M^{-1} in $CDCl_3$ and 370 ± 110 M^{-1} in toluene-d_8 at 298 K. For comparison, these association constants are on the same order as those determined by Müllen for similarly substituted hexa-*peri*-benzocoronenes (although those compounds were analyzed in terms of an indefinite association model).[9] Although the structural details are obviously quite different, the total aromatic surface area of **Tp(mP)$_2$Tp** is comparable to that of a hexabenzocoronene (e.g., 8 Clar sextets vs 7). Smaller aromatics related to **Tp(mP)$_2$Tp** exhibit much less tendency to aggregate; for example, 2,3,6,7-hexakis(*n*-hexyloxy)-triphenylene does not significantly associate under similar (solvent, temperature) conditions.[8] Other single-triphenylene-based compounds with expanded aromatic surfaces have been shown to aggregate, but with K_d values about 2 orders of magnitude smaller that those of **Tp(mP)$_2$Tp**.[35,36] While most of the reported triphenylene dimer macrocycles do exhibit

dx.doi.org/10.1021/jo501260c | J. Org. Chem. 2014, 79, 9009−9017

aggregation,[17,19−21,23] unfortunately there are none that have been studied under directly comparable conditions. That said, a macrocyclic triphenylene trimer reported by List and Müllen exhibits somewhat stronger aggregation behavior (indefinite association with K = 444 M^{-1} at 80 °C in TCE-d_2).

To better understand the self-association of **Tp(mP)$_2$Tp**, we also looked at the aggregation of two related compounds: the precursor **Tp(mP)$_2$** and tetrabenzocyclyne **B(mP)$_2$B**. Individually, these two compounds represent reasonable approximations of the structural components of **Tp(mP)$_2$Tp**. Like **Tp(mP)$_2$Tp**, the acyclic triphenylene **Tp(mP)$_2$** exhibits concentration-dependent ^{1}H chemical shifts in $CDCl_3$ (see the Supporting Information). Fitting of eq 1 to the data yields an association constant of K_d = 2.7 ± 0.7 M^{-1}, 2 orders of magnitude smaller than that for **Tp(mP)$_2$Tp**. No indication of aggregation was observed by NMR for the smaller macrocycle **B(mP)$_2$B**. Conversion of these K_d values to free energies of dimerization gives $\Delta G^\circ \approx 0$, −0.6, and −3.2 kcal/mol for **B(mP)$_2$B**, **Tp(mP)$_2$**, and **Tp(mP)$_2$Tp**, respectively. While not surprising, these results underscore the importance of both the area of the exposed aromatic-surface (**Tp(mP)$_2$** vs **B(mP)$_2$B**) and the preorganization as a symmetrical, rigid structure (**Tp(mP)$_2$Tp** vs **Tp(mP)$_2$**) in determining the favorability of columnar stacking of shape-persistent discotics.

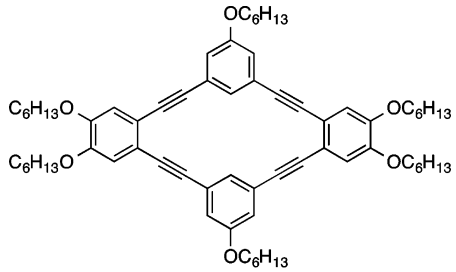

B(mP)$_2$B

For compounds with approximately circular shapes, the possible parallel stacking geometries are straightforward: they could stack in a perfect cofacial alignment, one component could be rotated relative to the other, and there could be a lateral displacement. In contrast, the possibilities for the dimers of oblong molecules like **Tp(mP)$_2$Tp** are more complex: rotation acts to decrease the area of contact of the two components, and there are two limiting modes of displacement (the long and short axes) that could act simultaneously. Understanding how this shape anisotropy affects the stacking modes of the dimers is an important question, however: as ever more complex molecular architectures are engineered into columnar materials, it may not always be possible (or desirable) to incorporate functional π-systems into cores with circular footprints.

It is clear from the changes in chemical shifts ($\Delta\delta$) in Figure 3 that the signals of some protons in **Tp(mP)$_2$Tp** are much more sensitive to dimerization than others (e.g., H_a vs H_d, H_g vs H_f). Presumably, these differences reflect the positioning of different protons with respect to the aromatic surface of the stacking partner. Indeed, this sensitivity of the chemical shifts of protons in different environments has been previously used in qualitative support of proposed stacking geometries.[35,37] The comparatively low symmetry of **Tp(mP)$_2$Tp**, with eight chemically inequivalent sets of protons, and the current availability of ab initio methods for NMR predictions[38] enable a straightforward semiquantitative exploration of its dimerization. Computational NMR predictions have been used to probe supramolecular structure in the past.[39−42] We are not aware of studies of the stacking of large discotics; however, NMR calculations of smaller stacked arenes have been previously reported. Notably, Czernek has shown that ab initio methods (including DFT methods) are able to provide a qualitative estimate of shielding tensors in benzene dimers, even if the methods do not themselves capture the energetics of the system.[43] This point is particularly relevant to the present case as the DFT methods used for NMR prediction do not predict the relevant aromatic stacking interactions. Similarly, Platts has used DFT (and other) methods to explore shielding parameters in parallel displaced and T-shaped benzene dimer configurations.[44]

For the **Tp(mP)$_2$Tp′** dimers, we carried out DFT calculations of the ^{1}H isotropic shieldings using the GIAO method[45,46] in combination with the WP04 functional[47] and 6-31G(d) basis set. This method offers an excellent balance between computational cost and accuracy.[48] The isotropic shieldings calculated for an isolated molecule of **Tp(mP)$_2$Tp′** (B3LYP/6-31G(d) geometry) are in very good agreement with the δ_m values of **Tp(mP)$_2$Tp**, as shown in the Supporting Information. The optimized geometry of **Tp(mP)$_2$Tp′** (Figure 1) was thus used as the basis for the construction of various dimers. Two macrocycles were held coplanar at a separation of 3.5 Å, chosen because of the 3.4−3.6 Å separation typically observed in simple stacked aromatics (e.g., in discotic liquid crystals[3] and stacked benzene dimers[49,50]). Various dimer geometries were then generated in three different ways: by displacing the macrocycles along their long axes by d_l, by displacing the macrocycles along their short axes by d_s, and by rotating the macrocycles relative to each other by θ, as shown in Figure 4 (top). As our interest was in qualitative trends, the dimer geometries were not themselves optimized.

Chemical shift changes on dimerization were then calculated ($\Delta\delta_{calc}$) by simply subtracting the calculated isotropic shieldings for the dimers from those calculated for the isolated **Tp(mP)$_2$Tp′**. The computational predictions (Figure 4, bottom) show a good match to the experimentally observed data in only one of the considered scenarios: of the 37 dimer geometries, the best 10% are those with $d_l \approx$ 3.0−4.5 Å, as judged by the RMS differences between the predicted and experimental values (RMS differences of ∼0.1 ppm). Considering the crudeness of the model adopted here, this agreement between the experimental and calculated $\Delta\delta$ values is remarkable: the long axis displacement alone semiquantitatively accounts for the chemical shift changes of each proton. The errors on the $\Delta\delta$ values are actually comparable to those typical of chemical shift calculations using fully optimized geometries.[48]

To confirm that the stacking stops at the dimer, we also carried out calculations on model trimers with variable long axis displacements; assuming that nearest neighbor effects predominate, the chemical shift changes for the central macrocycle in the trimer should be a reasonable approximation of those for a polymeric stack. These calculated chemical shift changes are wholly inconsistent with the experimental data (see the Supporting Information), with RMS differences of ≥0.35 ppm in all cases.

Of course, the results here do not preclude the formation of more complex dimers (i.e., combinations of d_l, d_s, and θ), but they do suggest that displacement along d_l is their defining structural characteristic. To further refine the results, we have

dx.doi.org/10.1021/jo501260c | J. Org. Chem. 2014, 79, 9009−9017

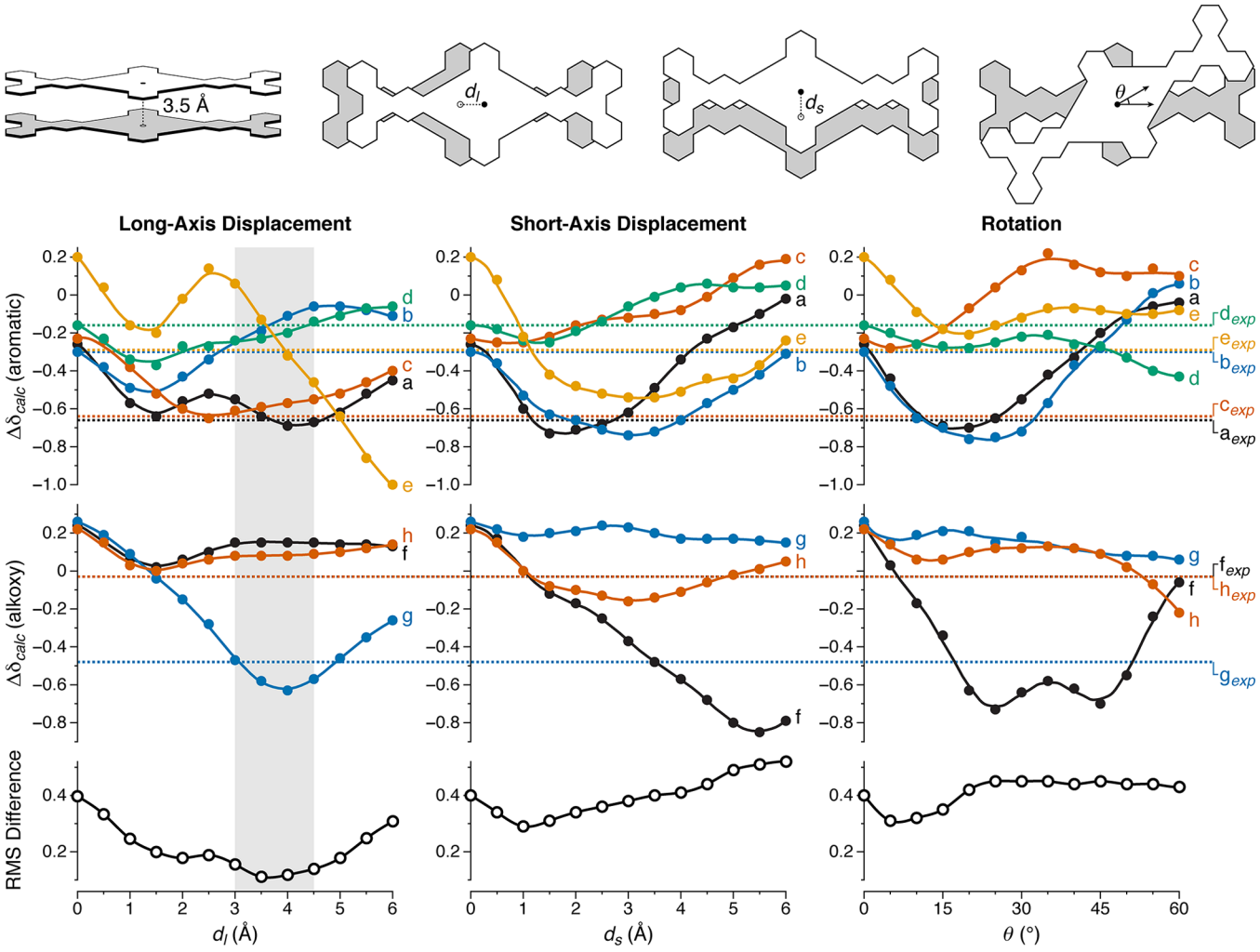

Figure 4. GIAO/PCM/WP04/6-31G(d) calculations of $\Delta\delta_{calc}$ values for model dimer systems. Top: Dimer geometries that were investigated. The macrocycles were held coplanar at a separation of 3.5 Å. The displacement along the long axis (d_l), the displacement along the short axis (d_s), and the relative orientation (θ) were varied. Middle: predicted $\Delta\delta_{calc}$ as a function of d_l, d_s, and θ. The experimental $\Delta\delta$ values for **Tp(mP)$_2$Tp** are represented by the dashed lines. Bottom: RMS differences between $\Delta\delta$ and $\Delta\delta_{calc}$, with the best matches highlighted in gray.

calculated the dependence of $\Delta\delta_{calc}$ on long axis displacement with other stacking distances ranging from 3.2−4.0 Å, with details given in the Supporting Information. While the stacking distance does affect $\Delta\delta_{calc}$, there is no effect on the general trend: the best fits to the experimental data are still found for $d_l \geq 3.5$ Å in all cases; the best match is obtained for a separation of 3.6 Å and d_l = 3.5 Å. Fixing the separation and d_l at these values, we then looked at the effect of varying d_s followed by θ. Short-axis displacement by d_s = 0.5 Å gave a small improvement in the RMS error (0.09 vs 0.10 ppm). Given that these RMS errors are comparable to the uncertainty inherent to the chemical shift calculations, this difference is probably best interpreted as uncertainty in the short-axis displacement on the order of 0−1 Å. The subsequent variation of θ did not improve the match to the experimental data, as perturbation by even 15° roughly doubled the RMS difference. The dimer geometry best matching the experimental data is shown in Figure 5.

In general, perfectly eclipsed, cofacial stacking of aromatic systems is not favorable. Even for the simplest system, the benzene dimer, parallel displaced stacks are favored (approximately isoenergetic with the T-shaped, edge-to-face configuration).[51] In order to understand the stacking of **Tp(mP)$_2$Tp**, we begin by focusing on the triphenylene moieties, as they

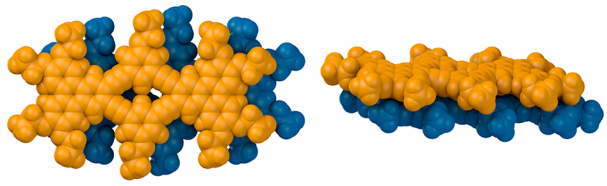

Figure 5. **Tp(mP)$_2$Tp′** dimer geometry with best match to experimental data. The two macrocycles are offset by d_l = 3.5 Å and d_s = 0.5 Å with a stacking distance of 3.6 Å.

represent the largest individual aromatic surfaces. Theoretical studies of the triphenylene dimer[52−54] have shown that the global energy minimum is obtained when the two molecules are related by a relative rotation of ∼35° along their C_3 axes.[52,54] For simple triphenylenes, parallel displacement (including that analogous to displacement by d_l) also generates local energy minima that are nearly isoenergetic with the rotated geometry. However, these minima are reached at a displacement of 1−2 Å for unsubstituted triphenylene, significantly less than the 3.5−4.0 Å observed here for **Tp(mP)$_2$Tp**.

The preference for lateral displacement (d_l) over rotation (θ) in **Tp(mP)$_2$Tp** is presumably a direct consequence of its

dx.doi.org/10.1021/jo501260c | J. Org. Chem. 2014, 79, 9009−9017

oblong shape: because of the rigid bridging *m*-phenylenes, one triphenylene cannot rotate with respect to its stacked partner without greatly decreasing the overall contact between the two molecules. In contrast, lateral displacement is obviously accommodated at both ends simultaneously. Why then is the observed displacement roughly a factor of 2 larger than can be explained by the triphenylenes alone? To explore these interactions further, we carried out a simple computational model study on the parallel-displaced stacking of 2,3,6,7-tetraethoxytriphenylene **6**. By analogy with the **Tp(mP)$_2$Tp′** dimers, its structure was optimized at the B3LYP/6-31G(d) level and dimers were constructed with a fixed interplanar separation of 3.5 Å, varying the displacement by analogy with d_l (Figure 4). As the purpose of these calculations was again a qualitative explanation of the trends, the geometries of the dimers were not themselves optimized. Single-point energies were calculated at the B97-D/TZV(2d,2p) level, which is widely used in the modeling of aromatic stacking interactions.[50,55,56] As shown in Figure 6, the optimum displacement

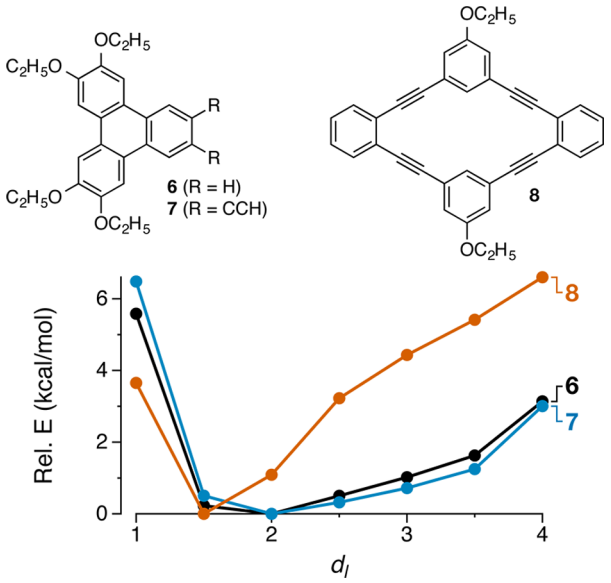

Figure 6. Energy profile for displacement along d_l for dimers of model compounds **6**–**8**. The stacking distance in the dimers is 3.5 Å.

is ∼2 Å, very close to that reported for the parent (unsubstituted) triphenylene, suggesting that the alkoxy groups do not account for the increased displacement in **Tp(mP)$_2$Tp** dimers through a simple electronic effect. We then considered the possibility that the extension of the π-surface into the macrocycle favors increased displacement. However, similar B97-D/TZV(2d,2p) calculations on 2,3,6,7-tetraethoxy-10,11-diethynyltriphenylene **7** suggest only an insignificant effect on the optimum d_l. Further calculations on the central TBC unit **8** suggest that it also favors displacements of 1.5–2.0 Å.[57] While these calculations are crude, they suggest that the displacement by d_l = 3.5–4.0 Å is not intrinsically favored by electronic effects on the aromatic stacking interactions responsible for dimer formation.

The simplest explanation for the observed stacking behavior is that the "extra" displacement is driven by steric interactions between the alkoxy side chains. It is notable that the dimer geometries best matching the experimental NMR data (e.g., Figure 5) place two of the three sets of side chains of one **Tp(mP)$_2$Tp** molecule in registry with the gaps along the periphery of the other molecule. These steric effects would not be captured by the DFT calculations because of the side-chain truncation to ethoxy groups and in particular because only rigid single conformers were considered. The fitting of the alkoxy groups of one molecule into the empty spaces of the other is qualitatively obvious from the NMR observations (Figure 3): H_f and H_h show very little change in chemical shift relative to the monomer ($\Delta\delta \approx 0$), indicating that they are out of contact with the aromatic surface of the stacking partner.

This explanation is consistent with the stacking behavior of related systems. For example, while the structures of columnar liquid crystals as a class typically involve tilting relative to the column axis[58] (implying some lateral displacement of the discotic cores), similar interactions are thought to occur between alkoxy groups in triphenylene-based liquid crystals.[59] Indeed, in the solid-state structures of simple hexaalkoxytriphenylenes, it is the alkoxy groups and their steric demand that dictate the packing arrangements, not stacking interactions between the triphenylenes.[60] Further, steric interactions between thioether side chains have been implicated in the helical twisting of the H phase of the well-known columnar semiconductor 2,3,6,7,10,11-hexahexylthiotriphenylene (HHTT).[61] The offset induced here is also reminiscent of Anthony and co-workers's use of bulky groups to control the crystal packing of pentacene derivatives.[62] The steric effects of substituents on discotic cores have been deliberately exploited to control self-assembly: Müllen and co-workers have used bulky substituents to direct the self-assembly of hexabenzocoronenes in solution, promoting the formation of twisted dimers.[37]

A common theme of these studies is that when substituents are radially distributed around a discotic core, the minimization of steric interactions naturally occurs via rotation, maintaining contact between the aromatic surfaces. It is also true that typical circular aromatic cores, including triphenylenes (as discussed above), hexabenzocoronenes, and phenylene ethynylene macrocycles,[63,64] tend to intrinsically favor twisted stacking geometries. Here, however, the **Tp(mP)$_2$Tp** molecules minimize interactions between the substituents through lateral displacement as a direct consequence of their elongated shapes, as this geometry best maintains contact between the aromatic surfaces. This effect occurs without any specific, directional intermolecular interactions (e.g., hydrogen bonds), which have been used to direct discotics toward alternate self-assembly modes in the past.[65] Moving forward, these results suggest that polymeric stacks of similar oblong discotics will maintain approximately rectangular geometries, over short length scales, as opposed to helical or rotationally disordered stacks with overall circular cross-sections.

■ CONCLUSIONS

In summary, we report here a new shape-persistent macrocycle, **Tp(mP)$_2$Tp**, with two triphenylenes bridged by *m*-phenylene units leading to a pronounced oblong shape. UV–vis and fluorescence spectroscopies suggest little electronic interaction between the two triphenylene moieties. In solution, the macrocycle aggregates into stacked dimers with association constants of K_d = 215 ± 5 M^{-1} (in $CDCl_3$) and 370 ± 110 M^{-1} (in toluene-d_8), as determined from the concentration dependence of ^{1}H NMR spectra. The association constants are higher than those reported for other shape-persistent macrocycles but comparable to other discotics with similar aromatic surface areas (e.g., hexa-*peri*-benzocoronenes). DFT

dx.doi.org/10.1021/jo501260c | J. Org. Chem. 2014, 79, 9009–9017

modeling was used to probe how various dimer geometries would affect the ^{1}H chemical shifts. Only displacement along the long axis of the dimer was in agreement with the experimental observations, with the optimum geometry corresponding to a stacking distance of 3.6 Å and a lateral displacement of 3.5−4.0 Å. The magnitude of this displacement cannot be explained by the intrinsic electronic stacking preferences of either the triphenylene units or the macrocyclic core but instead likely reflects the steric influence of the alkoxy side chains. This dimer geometry demonstrates that the oblong shape of the macrocycle has a significant effect on its self-assembly even absent specific, directional interactions.

EXPERIMENTAL SECTION

General Methods. Unless otherwise noted, all solvents, reagents, and starting materials were purchased from commercial sources and used without further purification. Melting points were determined using a differential scanning calorimeter at a heating rate of 10 °C/min. NMR spectra were measured in $CDCl_3$ solutions using 300 or 500 MHz NMR spectrometers. Chemical shifts are reported in δ (ppm) relative to TMS using the residual solvent protons as internal standards (7.28 ppm for ^{1}H, 77.0 for ^{13}C in $CDCl_3$ and 2.06, 205.3 ppm in acetone-d_6). MALDI-TOF mass spectra were recorded in reflectron mode using DHB as the matrix or without added matrix.

Synthesis of Macrocycle Tp(mP)$_2$Tp (Scheme 1). *2,3-Dibromo-6,7,10,11-tetramethoxytriphenylene (**2**).* A solution of 2,3,6,7-tetramethoxytriphenylene[25] (**1**) (2.07 g, 5.94 mmol) in CH_2Cl_2 (600 mL) was cooled in an ice−salt bath and then treated dropwise with Br_2 (1.87 g, 11.7 mmol). The mixture was stirred overnight at rt, treated with 20% NaS_2O_5(aq), and extracted with CH_2Cl_2. The organic layers were dried ($MgSO_4$), filtered, and concentrated. Purification by recrystallization ($CHCl_3$) gave compound **2** as a white solid (1.53 g, 51%): mp 286 °C; ^{1}H NMR (500 MHz, $CDCl_3$) δ 8.57 (s, 2H), 7.71 (s, 2H), 7.68 (s, 2H), 4.15 (s, 6H), 4.14 (s, 6H); ^{13}C NMR (500 MHz, $CDCl_3$) δ 150.1, 149.1, 129.2, 127.7, 124.3, 122.0, 121.6, 104.3, 104.0, 56.2, 56.1; MALDI-TOF-MS (no matrix) calcd for $C_{22}H_{18}Br_2O_4$ 505.96, found 505.87 (see the Supporting Information for theoretical and experimental isotopic distributions).

*2,3-Dibromo-6,7,10,11-tetrahydroxytriphenylene (**3**).* A solution of **2** (1.1 g, 2.2 mmol) in CH_2Cl_2 (150 mL) was cooled to −78 °C, treated with a 1 M solution of BBr_3 in CH_2Cl_2 (20 mL, 20 mmol), and stirred at rt for 18 h. The reaction mixture was poured into water and then extracted with EtOAc. The organic layers were dried ($MgSO_4$), filtered, and concentrated to give compound **10** (0.93 g, 95%) as a gray solid which was used without further purification: mp 140 °C dec; ^{1}H NMR (500 MHz, acetone-d_6) δ 8.74 (s, 2H), 8.04 (s, 2H), 7.89 (s, 2H), 3.18 (br s, 4H); ^{13}C NMR (500 MHz, $CDCl_3$) δ 147.1, 145.7, 129.7, 127.8, 124.5, 121.0, 120.9, 108.5, 108.0; MALDI-TOF-MS (DHB) calcd for $C_{18}H_{10}Br_2O_4$ 447.89, found 447.75 (see the Supporting Information for theoretical and experimental isotopic distributions).

*2,3-Dibromo-6,7,10,11-tetrahexyloxytriphenylene (**4**).* A mixture of **3** (81 mg, 0.18 mmol), 1-bromohexane (238 mg, 1.44 mol), and K_2CO_3 (249 mg, 1.8 mmol) in DMF (1 mL) was heated at reflux for 40 h. The solvents were then evaporated and washed with CH_2Cl_2. The solvents were evaporated, and the residue was partitioned between dilute H_2SO_4(aq) and CH_2Cl_2. The aqueous layer was extracted with CH_2Cl_2, and the combined organic layers were dried ($MgSO_4$), filtered, and concentrated. Purification by flash chromatography (2:1 hexanes/toluene) gave **4** (62.1 mg, 44%) as a white solid with the expected spectral properties.[25]

*Trimer **5**.* A Schlenk vacuum tube was charged with **4** (592 mg, 0.75 mmol), CuI (4.3 mg, 0.023 mmol), $Pd(OAc)_2$ (5.0 mg, 0.022 mmol), and PPh_3 (39.6 mg, 0.15 mmol). The tube was evacuated and backfilled with argon (3×), and then 1-ethynyl-3-(hexyloxy)-5-[(triisopropylsilyl)ethynyl]benzene[28] (789.3 mg, 2.06 mmol) was added as a solution in 1:3 triethylamine/toluene (40 mL). The reaction mixture was degassed by three freeze−pump−thaw cycles, sealed, and stirred at 80 °C for 24 h. The mixture was then diluted with EtOAc, washed with water and brine, dried ($MgSO_4$), filtered, and concentrated. Purification by flash chromatography (3:1 hexanes/CH_2Cl_2) gave **5** as a yellow solid (926 mg, 89%): mp 79 °C; ^{1}H NMR (500 MHz, $CDCl_3$) δ 8.64 (s, 2H), 7.96 (s, 2H), 7.81 (s, 2H), 7.39 (s, 2H), 7.11 (s, 2H), 7.02 (s, 2H), 4.3−4.2 (m, 8H), 3.86 (t, J = 6.4 Hz, 4H), 2.0−1.9 (m, 8H), 1.75 (qu, J = 7.4 Hz, 4H), 1.61 (m, 8H), 1.5−1.3 (m, 16H), 1.2−1.1 (m, 54H), 1.0−0.9 (m, 18H); ^{13}C NMR (500 MHz, $CDCl_3$) δ 158.9, 150.1, 149.3, 128.6, 127.4, 126.5, 124.84, 124.79, 124.3, 122.6, 122.3, 119.3, 117.0, 106.8, 106.1, 92.7, 91.1, 89.1, 69.6, 69.4, 68.2, 31.7, 31.6, 29.4, 29.3, 25.8, 25.7, 22.7, 22.6, 18.7, 14.1, 11.3; MALDI-TOF-MS (DHB) calcd for $C_{92}H_{132}O_6Si_2$ 1388.96, found 1388.83 (see the Supporting Information for theoretical and experimental isotopic distributions).

*Trimer **Tp(mP)$_2$**.* A solution of **5** (893.4 mg, 0.64 mmol) in THF (15 mL) was treated with a 1 M solution of TBAF in THF (369.7 mg, 1.41 mmol). The reaction mixture was stirred at rt, poured into water, and extracted with EtOAc. The combined organic layers were dried ($MgSO_4$), filtered, and concentrated. Purification by flash chromatography (2:1 hexanes/CH_2Cl_2) gave **Tp(mP)$_2$** (422.7 mg, 61%) as a light yellow solid: mp 85 °C; ^{1}H NMR (500 MHz, $CDCl_3$) δ 8.57 (s, 2H), 7.90 (s, 2H), 7.77 (s, 2H), 7.41 (s, 2H), 7.17 (s, 2H), 7.05 (s, 2H), 4.3−4.2 (m, 8H), 3.92 (t, J = 6.4 Hz, 4H), 3.09 (s, 2H), 2.0−1.9 (m, 8H), 1.79 (qu, J = 7.1 Hz, 4H), 1.6−1.5 (m, 8H), 1.5−1.3 (m, 28H), 1.0−0.9 (m, 18H); ^{13}C NMR (500 MHz, $CDCl_3$) δ 158.9, 150.1, 149.3, 128.6, 127.6, 126.6, 124.92, 124.88, 123.5, 122.6, 122.3, 119.0, 117.8, 106.75, 106.68, 92.4, 89.3, 82.8, 77.5, 69.6, 69.3, 68.2, 31.7, 31.6, 29.4, 29.2, 25.9, 25.88, 25.86, 22.7, 22.6, 14.08, 14.06; MALDI-TOF-MS (DHB) calcd for $C_{74}H_{92}O_6$ 1076.69, found 1076.55 (see the Supporting Information for theoretical and experimental isotopic distributions).

*Macrocycle **Tp(mP)$_2$Tp**.* A Schlenk vacuum tube was charged with $Pd(P^tBu_3)_2$ (6.7 mg, 0.013 mmol) and **4** (150 mg, 0.19 mmol), evacuated, and backfilled with argon (3×). Then **Tp(mP)$_2$** (137 mg, 0.13 mmol) was added as a solution in 1:3 triethylamine/toluene (16 mL). The reaction mixture was degassed by three freeze−pump−thaw cycles and stirred at room temperature for 18 h. The reaction mixture was then diluted with toluene, washed with water, dried ($MgSO_4$), filtered, and concentrated. Purification by flash chromatography (2:1 hexanes/CH_2Cl_2) gave **Tp(mP)$_2$Tp** (34 mg, 16%) as a white solid: mp 80 °C; ^{1}H NMR (500 MHz, $CDCl_3$) δ 8.31 (s, 4H), 7.86 (s, 4H), 7.65 (s, 2H), 7.46 (s, 4H), 7.18 (s, 4H), 4.36 (br t, 8H), 4.14 (br t, 4H), 3.99 (br t, 8H), 2.06 (m, 8H), 1.93 (m, 16H), 1.71 (m, 8H), 1.6−1.4 (m, 48H), 1.0−0.9 (m, 30H); ^{13}C NMR (500 MHz, $CDCl_3$) δ 158.9, 149.8, 149.0, 128.5, 128.4, 126.6, 124.9, 124.5, 122.4, 121.9, 117.3, 106.8, 105.9, 92.2, 89.5, 69.3, 69.1, 68.4, 31.9, 31.78, 31.75, 29.7, 29.5, 29.4, 26.1, 25.9, 22.8, 22.7, 14.14, 14.09; MALDI-TOF-MS (DHB) calcd for $C_{116}H_{148}O_{10}$ 1701.11, found 1700.96 (see the Supporting Information for theoretical and experimental isotopic distributions).

Synthesis of Macrocycle B(mP)$_2$B (Scheme 2). The synthesis of macrocycle **B(mP)$_2$B** is shown in Scheme 2.

*Trimer **9**.* A Schlenk vacuum tube was charged with CuI (3.8 mg, 0.02 mmol), $Pd(OAc)_2$ (5.6 mg, 0.02 mmol), and PPh_3 (32.0 mg, 0.12 mmol), and the tube was evacuated and backfilled with argon (3 ×). Then 1-ethynyl-3-(hexyloxy)-5-[(triisopropylsilyl)ethynyl)]benzene[28] (246.3 mg, 0.64 mmol) and 1,2-bis(hexyloxy)-4,5-diiodobenzene[66] (167.4 mg, 0.32 mmol) were added as solutions in diisopropylamine (1.6 mL). The suspension was degassed by three freeze−pump−thaw cycles and stirred overnight at 80 °C. The reaction mixture was then cooled to rt, diluted with EtOAc, and washed with water and brine. The combined aqueous layers were extracted with EtOAc, and then the combined organic layers were dried ($MgSO_4$), filtered, and concentrated. Purification by flash chromatography (1:2 CH_2Cl_2/hexanes) gave 206.1 mg (63%) of **9** as a reddish-orange viscous oil, which solidified on standing at rt: ^{1}H NMR (300 MHz, $CDCl_3$) δ 7.23 (~t, 2H), 6.99 (s, 2H), 6.97 (~t, 2H), 6.94 (~t, 2H), 4.02 (t, J = 6.5 Hz, 4H), 3.79 (t, J = 6.3 Hz, 4H), 1.84 (qu, J = 6.8 Hz, 4H), 1.70 (qu, J = 6.5 Hz, 4H), 1.48 (m, 4H), 1.35 (m, 20H), 1.10 (s, 42H), 0.90 (m,

dx.doi.org/10.1021/jo501260c | J. Org. Chem. 2014, 79, 9009−9017

Scheme 2[a]

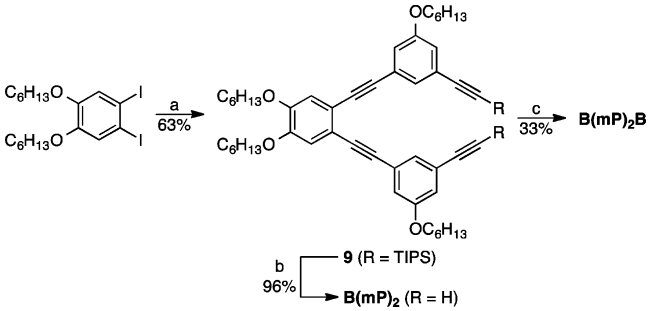

[a]Reagents and conditions: (a) 1-ethynyl-3-(hexyloxy)-5-[(triisopropylsilyl)ethynyl)]benzene, $Pd(OAc)_2$, CuI, PPh_3, N^iPr_3, 80 °C; (b) TBAF, THF, rt; (c) $Pd(P^tBu_3)_2$, DABCO, toluene, rt.

12H); ^{13}C NMR (75 MHz, $CDCl_3$) δ 159.2, 150.0, 127.6, 125.1, 125.0, 119.3, 117.6, 117.0, 106.7, 91.8, 91.2, 89.0, 69.8, 68.6, 31.8, 29.4, 25.9, 22.7, 18.8, 14.0, 11.7; MALDI-TOF-MS (dithranol) calcd for $C_{68}H_{102}O_4Si_2$ 1038.73, found 1038.67 (see the Supporting Information for theoretical and experimental isotopic distributions).

Trimer ***B(mP)$_2$.*** To a solution of **9** (168.5 mg, 0.16 mmol) in THF (4 mL) under an argon atmosphere was added a 1 M solution of TBAF in THF (0.11 mL, 0.11 mmol). The solution was stirred for 2 h at rt, diluted with EtOAc, and washed with water and brine. The combined aqueous layers were extracted with EtOAc, and then the combined organic layers were dried ($MgSO_4$), filtered, and concentrated. Purification by flash chromatography (1:3 CH_2Cl_2/hexanes) gave 113.2 mg (96%) of **B(mP)$_2$** as a yellow powder: ^{1}H NMR (300 MHz, $CDCl_3$) δ 7.26 (s, 2H), 7.03 (s, 2H), 7.00 (s, 2H), 6.97 (s, 2H), 4.03 (t, J = 6.7 Hz, 4H), 3.87 (t, J = 6.6 Hz, 4H), 3.03 (s, 2H), 1.84 (qu, J = 6.9 Hz, 4H), 1.73 (qu, J = 6.8 Hz, 4H), 1.41 (m, 24H), 0.91 (m, 12H); ^{13}C NMR (75 MHz, $CDCl_3$) δ 159.3, 150.2, 127.9, 125.3, 123.8, 119.3, 119.2, 118.4, 117.4, 91.7, 89.3, 83.3, 77.3, 70.0, 68.8, 31.8, 29.5, 29.5, 25.9, 22.7, 14.0; MALDI-TOF-MS (DHB) calcd for $C_{50}H_{62}O \sim 4$ (M^+) 726.46, found 726.37 (see the Supporting Information for theoretical and experimental isotopic distributions); HRMS (ESI) calcd for $C_{50}H_{63}O_4$ ($M + H^+$) 727.4726, found 727.4722.

Macrocycle ***B(mP)$_2$B.*** A Schlenk vacuum tube was charged with $Pd(P^tBu_3)_2$ (3.6 mg, 0.007 mmol) and **B(mP)$_2$** (34.1 mg, 0.047 mmol), and the tube evacuated and backfilled with argon (3×). Then DABCO (5.526 g, 49.264 mmol) and 1,2-bis(hexyloxy)-4,5-diiodobenzene (31.1 mg, 0.059 mmol) were added as a mixture in toluene (24.0 mL). The mixture was degassed by three freeze–pump–thaw cycles. After sonication to give a homogeneous solution, the reaction mixture was stirred at rt overnight. The solution was then diluted with toluene and washed with water and brine. The combined aqueous layers were extracted with toluene. Then the combined organics were dried ($MgSO_4$), filtered, and concentrated. Purification by flash chromatography (1:1 toluene/hexanes to 7:3 toluene:hexanes) gave 15.5 mg (33%) of **B(mP)$_2$B** as a light brown solid which was recrystallized from benzene to give an off-white powder prior to characterization: mp 183 °C; ^{1}H NMR (500 MHz, $CDCl_3$) δ 7.58 (s, 2H), 7.04 (s, 4H), 7.02 (s, 4H), 4.04 (t, J = 6.54 Hz, 8H), 4.00 (t, J = 6.4 Hz, 4H), 1.85 (qu, J = 7.1 Hz, 8H), 1.76 (m, 4H), 1.49 (m, 12H), 1.36 (m, 24H), 0.92 (~t, 18H); ^{13}C NMR (125 MHz, $CDCl_3$) δ 159.1, 149.5, 128.1, 124.8, 118.7, 117.2, 116.0, 91.6, 89.1, 69.4, 68.4, 31.7, 29.3, 29.2, 25.8, 25.8, 22.8, 14.2; MALDI-TOF-MS (DHB) calcd for $C_{68}H_{88}O_6$ 1000.66, found 1000.55 (see the Supporting Information for theoretical and experimental isotopic distributions).

UV–vis and Fluorescence Spectra. UV–vis and fluorescence spectra were determined in spectrophotometric-grade solvents used without further purification. UV–vis spectra were recorded using 10 mm quartz cuvettes (except in quantum yield measurements, for which 100 mm cuvettes were used). Emission spectra are corrected. Quantum yields were determined in nitrogen-sparged solutions relative to 9,10-diphenylanthracene in cyclohexane (Φ = 0.92), which was cross-checked against quinine bisulfate in 0.5 M H_2SO_4(aq) (Φ = 0.54), matching the literature values within 10%. The absorbance of the sample solutions was kept below 0.1 (10 mm cuvette) to avoid the inner filter effect. Measurements were performed at rt, with both sample and reference solutions excited at 350 nm. Fluorescence lifetimes were determined for nitrogen-sparged solutions by time-correlated single-photon counting. Good monoexponential fits were obtained for both **Tp(mP)$_2$Tp** and **Tp(mP)$_2$**.

Computational Chemistry. All calculations were performed using Gaussian 09, rev. B.01.[67] All energy minima were verified to have 0 imaginary frequencies by vibrational frequency analysis. Geometries are provided in the Supporting Information.

■ ASSOCIATED CONTENT

Ⓢ Supporting Information

Details of computational results (including geometries); NMR concentration-dependence plots and curve fitting; NMR predictions; NMR and mass spectra of synthesized compounds. This material is available free of charge via the Internet at http://pubs.acs.org.

■ AUTHOR INFORMATION

Corresponding Author

*E-mail: scott.hartley@miamioh.edu.

Notes

The authors declare no competing financial interest.

■ ACKNOWLEDGMENTS

This work was supported by the Air Force Office of Scientific Research (FA9550-10-1-0377) with additional support from the National Science Foundation (CHE-1306437).

■ REFERENCES

(1) Maggini, L.; Bonifazi, D. *Chem. Soc. Rev.* **2012**, *41*, 211–241.
(2) Babu, S. S.; Praveen, V. K.; Ajayaghosh, A. *Chem. Rev.* **2014**, *114*, 1973–2129.
(3) Laschat, S.; Baro, A.; Steinke, N.; Giesselmann, F.; Hägele, C.; Scalia, G.; Judele, R.; Kapatsina, E.; Sauer, S.; Schreivogel, A.; Tosoni, M. *Angew. Chem., Int. Ed.* **2007**, *46*, 4832–4887.
(4) Kaafarani, B. R. *Chem. Mater.* **2011**, *23*, 378–396.
(5) Chen, Z.; Lohr, A.; Saha-Möller, C. R.; Würthner, F. *Chem. Soc. Rev.* **2009**, *38*, 564–584.
(6) Würthner, F.; Kaiser, T. E.; Saha-Möller, C. R. *Angew. Chem., Int. Ed.* **2011**, *50*, 3376–3410.
(7) De Greef, T. F. A.; Smulders, M. M. J.; Wolffs, M.; Schenning, A. P. H. J.; Sijbesma, R. P.; Meijer, E. W. *Chem. Rev.* **2009**, *109*, 5687–5754.
(8) Gallivan, J. P.; Schuster, G. B. *J. Org. Chem.* **1995**, *60*, 2423–2429.
(9) Kastler, M.; Pisula, W.; Wasserfallen, D.; Pakula, T.; Müllen, K. *J. Am. Chem. Soc.* **2005**, *127*, 4286–4296.
(10) Würthner, F.; Thalacker, C.; Diele, S.; Tschierske, C. *Chem.—Eur. J.* **2001**, *7*, 2245–2253.
(11) Shetty, A. S.; Zhang, J.; Moore, J. S. *J. Am. Chem. Soc.* **1996**, *118*, 1019–1027.
(12) Höger, S.; Bonrad, K.; Mourran, A.; Beginn, U.; Möller, M. *J. Am. Chem. Soc.* **2001**, *123*, 5651–5659.
(13) Tobe, Y.; Utsumi, N.; Kawabata, K.; Nagano, A.; Adachi, K.; Araki, S.; Sonoda, M.; Hirose, K.; Naemura, K. *J. Am. Chem. Soc.* **2002**, *124*, 5350–5364.
(14) Zhao, D.; Moore, J. S. *Chem. Commun.* **2003**, 807–818.
(15) Leu, W. C. W.; Fritz, A. E.; Digianantonio, K. M.; Hartley, C. S. *J. Org. Chem.* **2012**, *77*, 2285–2298.
(16) Leu, W. C. W.; Hartley, C. S. *Org. Lett.* **2013**, *15*, 3762–3765.
(17) Wang, D.; Hsu, J. F.; Bagui, M.; Dusevich, V.; Wang, Y.; Liu, Y.; Holder, A. J.; Peng, Z. *Tetrahedron Lett.* **2009**, *50*, 2147–2149.

(18) Chou, C.; Wang, D.; Hsu, J. F.; Liu, Y.; Peng, Z. *Synth. Met.* **2009**, *159*, 1657−1663.
(19) Dutta, T.; Che, Y.; Zhong, H.; Laity, J. H.; Dusevich, V.; Murowchick, J. B.; Zang, L.; Peng, Z. *RSC Adv.* **2013**, *3*, 6008−6015.
(20) Zhang, L.; Hughes, D. L.; Cammidge, A. N. *J. Org. Chem.* **2012**, *77*, 4288−4297.
(21) Gopee, H.; Kong, X.; He, Z.; Chambrier, I.; Hughes, D. L.; Tizzard, G. J.; Coles, S. J.; Cammidge, A. N. *J. Org. Chem.* **2013**, *78*, 9505−9511.
(22) Schwab, M. G.; Qin, T.; Pisula, W.; Mavrinskiy, A.; Feng, X.; Baumgarten, M.; Kim, H.; Laquai, F.; Schuh, S.; Trattnig, R.; List, E. J. W.; Müllen, K. *Chem.—Asian. J.* **2011**, *6*, 3001−3010.
(23) Wettach, H.; Höger, S.; Chaudhuri, D.; Lupton, J. M.; Liu, F.; Lupton, E. M.; Tretiak, S.; Wang, G.; Li, M.; De Feyter, S.; Fischer, S.; Förster, S. *J. Mater. Chem.* **2011**, *21*, 1404−1415.
(24) Borner, R. C.; Jackson, R. F. W. *J. Chem. Soc., Chem. Commun.* **1994**, 845−846.
(25) Cammidge, A. N.; Gopee, H. *J. Mater. Chem.* **2001**, *11*, 2773−2783.
(26) Henderson, P.; Kumar, S.; Rego, J. A.; Ringsdorf, H.; Schuhmacher, P. *J. Chem. Soc., Chem. Commun.* **1995**, 1059−1060.
(27) Ichihara, M.; Suzuki, H.; Mohr, B.; Ohta, K. *Liq. Cryst.* **2007**, *34*, 401−410.
(28) Grave, C.; Lentz, D.; Schäfer, A.; Samorì, P.; Rabe, J. P.; Franke, P.; Schlüter, A. D. *J. Am. Chem. Soc.* **2003**, *125*, 6907−6918.
(29) Soheili, A.; Albaneze-Walker, J.; Murry, J. A.; Dormer, P. G.; Hughes, D. L. *Org. Lett.* **2003**, *5*, 4191−4194.
(30) Unfortunately, we were unable to probe interactions between the triphenylene units electrochemically, as both **Tp(mP)$_2$Tp** and **Tp(mP)$_2$** decomposed during attempts at cyclic voltammetry.
(31) The quantum yields are the same within experimental error.
(32) Unfortunately, NMR experiments in more polar solvents were not possible because **Tp(mP)$_2$Tp** was insufficiently soluble.
(33) Martin, R. B. *Chem. Rev.* **1996**, *96*, 3043−3064.
(34) Mitchell, P. R.; Sigel, H. *Eur. J. Biochem.* **1978**, *88*, 149−154.
(35) Lavigueur, C.; Foster, E. J.; Williams, V. E. *J. Am. Chem. Soc.* **2008**, *130*, 11791−11800.
(36) Lynett, P. T.; Maly, K. E. *Org. Lett.* **2009**, *11*, 3726−3729.
(37) Wu, J.; Fechtenkötter, A.; Gauss, J.; Watson, M. D.; Kastler, M.; Fechtenkötter, C.; Wagner, M.; Müllen, K. *J. Am. Chem. Soc.* **2004**, *126*, 11311−11321.
(38) Lodewyk, M. W.; Siebert, M. R.; Tantillo, D. J. *Chem. Rev.* **2012**, *112*, 1839−1862.
(39) Ajami, D.; Iwasawa, T.; Rebek, J., Jr. *Proc. Natl. Acad. Sci. U.S.A.* **2006**, *103*, 8934−8936.
(40) Klärner, F.-G.; Kahlert, B.; Nellesen, A.; Zienau, J.; Ochsenfeld, C.; Schrader, T. *J. Am. Chem. Soc.* **2006**, *128*, 4831−4841.
(41) Chelli, S.; Majdoub, M.; Jouini, M.; Aeiyach, S.; Maurel, F.; Chane-Ching, K. I.; Lacaze, P.-C. *J. Phys. Org. Chem.* **2007**, *20*, 30−43.
(42) Mugridge, J. S.; Bergman, R. G.; Raymond, K. N. *J. Am. Chem. Soc.* **2011**, *133*, 11205−11212.
(43) Czernek, J. *J. Phys. Chem. A* **2003**, *107*, 3952−3959.
(44) Platts, J. A.; Gkionis, K. *Phys. Chem. Chem. Phys.* **2009**, *11*, 10331−10339.
(45) Ditchfield, R. *Mol. Phys.* **1974**, *27*, 789−807.
(46) Wolinski, K.; Hinton, J. F.; Pulay, P. *J. Am. Chem. Soc.* **1990**, *112*, 8251−8260.
(47) Wiitala, K. W.; Hoye, T. R.; Cramer, C. J. *J. Chem. Theory Comput.* **2006**, *2*, 1085−1092.
(48) Jain, R.; Bally, T.; Rablen, P. R. *J. Org. Chem.* **2009**, *74*, 4017−4023.
(49) Sinnokrot, M. O.; Sherrill, C. D. *J. Phys. Chem. A* **2004**, *108*, 10200−10207.
(50) Wheeler, S. E. *J. Am. Chem. Soc.* **2011**, *133*, 10262−10274.
(51) Sinnokrot, M. O.; Sherrill, C. D. *J. Phys. Chem. A* **2006**, *110*, 10656−10668.
(52) Yurtsever, E. *Theor. Chem. Acc.* **2010**, *127*, 133−139.
(53) Cinacchi, G.; Prampolini, G. *J. Phys. Chem. C* **2008**, *112*, 9501−9509.
(54) Mikołajczyk, M. M.; Toman, P.; Bartkowiak, W. *Chem. Phys. Lett.* **2010**, *485*, 253−257.
(55) Vázquez-Mayagoitia, Á.; Sherrill, C. D.; Aprà, E.; Sumpter, B. G. *J. Chem. Theory Comput.* **2010**, *6*, 727−734.
(56) Grimme, S.; Antony, J.; Schwabe, T.; Mück-Lichtenfeld, C. *Org. Biomol. Chem.* **2007**, *5*, 741−758.
(57) These same single-point calculations were also carried out for the full **Tp(mP)$_2$Tp** dimer geometries used for the NMR calculations. The results are equivalent to those of just the central macrocyclic portion.
(58) Chandrasekhar, S. Columnar, Discotic Nematic and Lamellar Liquid Crystals: Their Structures and Physical Properties. In *Handbook of Liquid Crystals*; Demus, D., Goodby, J. W., Gray, G. W., Spiess, H.-W., Vill, V., Eds.; Wiley-VCH: New York, 1998; pp 749−780.
(59) Cotrait, M.; Marsau, P.; Pesquer, M.; Volpilhac, V. *J. Phys. (Paris)* **1982**, *43*, 355−359.
(60) Andresen, T. L.; Krebs, F. C.; Thorup, N.; Bechgaard, K. *Chem. Mater.* **2000**, *12*, 2428−2433.
(61) Fontes, E.; Heiney, P. A.; de Jeu, W. H. *Phys. Rev. Lett.* **1988**, *61*, 1202−1205.
(62) Anthony, J. E.; Brooks, J. S.; Eaton, D. L.; Parkin, S. R. *J. Am. Chem. Soc.* **2001**, *123*, 9482−9483.
(63) Wheeler, S. E. *CrystEngComm* **2012**, *14*, 6140−6145.
(64) Ng, M.-F.; Yang, S.-W. *J. Phys. Chem. B* **2007**, *111*, 13886−13893.
(65) Ikeda, M.; Takeuchi, M.; Shinkai, S. *Chem. Commun.* **2003**, 1354−1355.
(66) Balandina, T.; Tahara, K.; Sändig, N.; Blunt, M. O.; Adisoejoso, J.; Lei, S.; Zerbetto, F.; Tobe, Y.; De Feyter, S. *ACS Nano* **2012**, *6*, 8381−8389.
(67) Frisch, M. J.; Trucks, G. W.; Schlegel, H. B.; Scuseria, G. E.; Robb, M. A.; Cheeseman, J. R.; Scalmani, G.; Barone, V.; Mennucci, B.; Petersson, G. A.; Nakatsuji, H.; Caricato, M.; Li, X.; Hratchian, H. P.; Izmaylov, A. F.; Bloino, J.; Zheng, G.; Sonnenberg, J. L.; Hada, M.; Ehara, M.; Toyota, K.; Fukuda, R.; Hasegawa, J.; Ishida, M.; Nakajima, T.; Honda, Y.; Kitao, O.; Nakai, H.; Vreven, T.; Montgomery, J. A., Jr.; Peralta, J. E.; Ogliaro, F.; Bearpark, M.; Heyd, J. J.; Brothers, E.; Kudin, K. N.; Staroverov, V. N.; Keith, T.; Kobayashi, R.; Normand, J.; Raghavachari, K.; Rendell, A.; Burant, J. C.; Iyengar, S. S.; Tomasi, J.; Cossi, M.; Rega, N.; Millam, J. M.; Klene, M.; Knox, J. E.; Cross, J. B.; Bakken, V.; Adamo, C.; Jaramillo, J.; Gomperts, R.; Stratmann, R. E.; Yazyev, O.; Austin, A. J.; Cammi, R.; Pomelli, C.; Ochterski, J. W.; Martin, R. L.; Morokuma, K.; Zakrzewski, V. G.; Voth, G. A.; Salvador, P.; Dannenberg, J. J.; Dapprich, S.; Daniels, A. D.; Farkas, O.; Foresman, J. B.; Ortiz, J. V.; Cioslowski, J.; Fox, D. J. *Gaussian 09*, Rev. B.01; Gaussian, Inc.: Wallingford, CT, 2010.